

Quantum phases of canted dipolar bosons in a two-dimensional square optical lattice

Soumik Bandyopadhyay ^{1,2}, Rukmani Bai,¹ Sukla Pal,^{1,3} K. Suthar,^{1,4} Rejish Nath ⁵ and D. Angom ^{1,*}

¹Physical Research Laboratory, Ahmedabad 380009, Gujarat, India

²Indian Institute of Technology Gandhinagar, Palaj, Gandhinagar 382355, Gujarat, India

³Department of Physics, Centre for Quantum Science, and Dodd-Walls Centre for Photonic and Quantum Technologies, University of Otago, Dunedin 9016, New Zealand

⁴Instytut Fizyki imienia Mariana Smoluchowskiego, Uniwersytet Jagielloński, ulica Łojasiewicza 11, 30-348 Kraków, Poland

⁵Indian Institute of Science Education and Research, Pune 411008, India



(Received 9 July 2019; revised manuscript received 20 October 2019; published 25 November 2019)

We consider a minimal model to describe the quantum phases of ultracold dipolar bosons in two-dimensional square optical lattices. The model is a variation of the extended Bose-Hubbard model and apt to study the quantum phases arising from the variation in the tilt angle θ of the dipolar bosons. At low tilt angles, $0^\circ \leq \theta \lesssim 25^\circ$, the ground states of the system are phases with checkerboard order, which can be either checkerboard supersolids or checkerboard density waves. For high tilt angles, $35^\circ \lesssim \theta \lesssim 55^\circ$, phases with striped order of the supersolid or density wave are preferred. In the intermediate domain, $25^\circ \lesssim \theta \lesssim 35^\circ$, an emulsion or superfluid phase intervenes the transition between the checkerboard and the striped phases. The attractive interaction dominates at $\theta \gtrsim 55^\circ$, which renders the system unstable, and there is a density collapse. For our studies we use Gutzwiller mean-field theory to obtain the quantum phases and the phase boundaries. In addition, we calculate the phase boundaries between an incompressible and a compressible phase of the system by considering second-order perturbation analysis of the mean-field theory. The analytical results, where applicable, are in excellent agreement with the numerical results. In our study, the incompressible phases have an average occupancy per site $\rho \leq 1$, but the compressible phases can have $\rho > 1$.

DOI: [10.1103/PhysRevA.100.053623](https://doi.org/10.1103/PhysRevA.100.053623)

I. INTRODUCTION

In the strongly interacting regime, neutral bosons with short-range interactions in optical lattices exhibit two quantum phases: Mott insulator (MI) and superfluid (SF) [1–4]. A prototypical model that describes the properties of such systems is the Bose-Hubbard model (BHM) [1,2,5]. The model considers nearest-neighbor (NN) hopping and on-site contact interaction between the bosons. The strength of the on-site interaction is determined by the s -wave scattering length, which is a real quantity for bosonic atoms. And it must be positive to prevent collapse. The BHM is, however, not suitable to describe quantum phases which have off-site density-density correlations, such as the density wave (DW) and supersolid (SS) [6–13]. The emergence of these quantum phases and their stabilization require long-range interactions. The interaction can be a dipole-dipole interaction [10,12–15], a fermion-mediated boson-boson interaction in Bose-Fermi mixtures [16], etc. The former is realized in dipolar atoms like Cr [17–19], Dy [20,21], and Er [22,23] and polar molecules [24–29]. So, an extension of the BHM accounting for the dipole-dipole interaction can harbor the above phases. But it is important to note that the on-site interaction in the BHM for reactive polar molecules has to be treated differently, as the scattering length is a complex quantity [30,31]. And a large number of Fano-Feshbach resonances in ultracold

collisions of nonreactive polar molecules [32–34] modify the single-channel contact interaction pseudopotential of the BHM [35–37], which in turn modifies the phase diagram [38]. In this work, we do not consider these aspects of polar molecules, which require further investigation. Apart from quantum phases in optical lattices, dipolar bosons, specifically polar molecules, offer fast and robust schemes for quantum computation [39–41]. In addition, the long-range and anisotropic nature of the dipole-dipole interaction can induce exotic magnetic orders. Thus, these systems are promising simulators for quantum magnetism [42–45].

The BHM with the nearest-neighbor lattice site interparticle interaction and its variations is referred to as the extended Bose-Hubbard model [46,47]. It is a minimal model which harbors phases with off-site density-density correlations. Based on this model several theoretical studies have analyzed the equilibrium phases of bosons in optical lattices and their stability properties [48–54] and the dynamics of quantum phase transitions by quenching system parameters [55,56]. In two dimensions this is equivalent to a dipole-dipole interaction limited to the NN interaction and with the dipoles aligned perpendicular to the lattice plane. And such systems exhibit checkerboard order in the DW and SS phases. Thus, a minimal model to describe quantum phases of dipolar bosons in optical lattices is to limit the interaction to NNs. This is the system we consider in the present work. In previous studies, the quantum phases of lattice bosons with anisotropic dipolar interaction and their stability have been analyzed [10,12,13]. In addition, the phase diagrams for dipolar bosons in a

*angomd@gmail.com

two-dimensional (2D) square optical lattice with staggered flux in the minimal model have been studied [57]. A recent work [58] reported the equilibrium phases of hard-core dipolar bosons at half-filling in a 2D optical lattice with variation of the tilt angle. And it reported a DW phase with checkerboard and striped order. However, the experimental observations are in the soft-core regime [23]. In this experiment Baier *et al.* [23] realized the BHM for strongly magnetic Er atoms in a 3D optical lattice and observed the NN interaction as a genuine consequence of the long-range dipolar interactions. And they also varied the tilt angle of dipolar atoms to examine the effect of an anisotropic dipole-dipole interaction on the SF-MI phase transition.

Motivated by the experimental realization, we investigate the quantum phases of canted soft-core dipolar bosons in a 2D square optical lattice. Hence, our work addresses a key research gap in the physics of soft-core dipolar bosons in a strongly interacting domain. We show that the system exhibits compressible checkerboard SS (CBSS) and striped SS (SSS) phases in addition to incompressible checkerboard DW (CBDW) and striped DW (SDW) phases. It is to be noted that the SS phases are absent in the hard-core regime [58]. In addition, the dipolar interaction in the soft-core regime leads to a multitude of DW phases with average occupation number $\rho \geq 1$. This is in contrast to the hard-core regime, where DW phases have $\rho < 1$. In this work, the parameters chosen are such that the incompressible phases have $\rho \leq 1$ and this is the most relevant regime for experiments [23]. But the compressible phases, such as SF and SS, can have $\rho \geq 1$.

We have organized the remainder of this article as follows. In Sec. II we discuss the zero-temperature Hamiltonian of the minimal model. Section III provides a brief account of the Gutzwiller mean-field (MF) theory and the quantum phases of the model. Then we discuss the mean-field decoupling theory to calculate the compressible-incompressible phase boundaries analytically. Section IV describes the numerical procedures adopted to solve the model. The phase diagrams and key results of our work are discussed in Sec. V. We conclude in Sec. VI.

II. THEORETICAL MODEL

We consider charge neutral, polarized dipolar bosons loaded in a 2D square optical lattice with lattice constant a . At zero temperature, the physics of such a system is well described by the lowest band BHM with dipolar interaction. The grand canonical Hamiltonian of the system is [1,10–13]

$$\hat{H} = -J \sum_{\langle ij \rangle} (\hat{b}_i^\dagger \hat{b}_j + \text{H.c.}) - \sum_i \mu \hat{n}_i + \hat{H}_I, \quad (1)$$

where $i \equiv (p, q)$ and $j \equiv (p', q')$ denote the lattice indices, \hat{b}_i (\hat{b}_i^\dagger) and \hat{n}_i are the bosonic annihilation (creation) and occupation number operators, and $\langle \dots \rangle$ denotes the sum over NN lattice sites. In addition, J and μ are the strength of the hopping and chemical potentials, respectively. The latter term is the interatomic interaction Hamiltonian

$$\hat{H}_I = \sum_i \frac{U}{2} \hat{n}_i (\hat{n}_i - 1) + \frac{C_{dd}}{2} \sum_{ij} \hat{n}_i \hat{n}_j \frac{(1 - 3\cos^2 \alpha_{ij})}{|\vec{r}_j - \vec{r}_i|^3}, \quad (2)$$

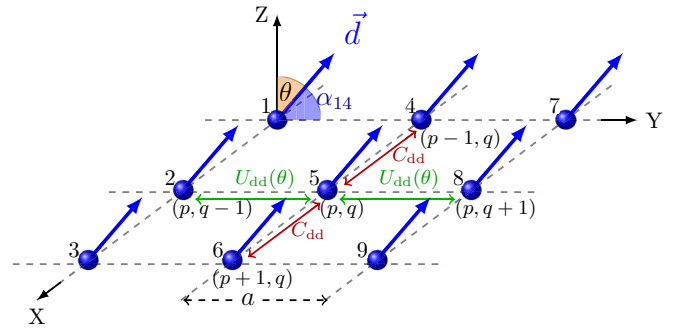


FIG. 1. Schematics of dipolar bosons in a two-dimensional square optical lattice with dipolar interaction among the bosons at nearest-neighbor lattice sites. We consider the dipoles to be polarized in the y - z plane and the angle subtended by the direction of the dipole moments (polarization axis) with the z axis is the tilt angle θ . The tilt angle is illustrated by the orange-shaded sector. The angle between the polarization axis and the vector $(\vec{r}_4 - \vec{r}_1)$, α_{14} , is represented by the blue-shaded sector. The dipolar interaction between bosons at lattice sites (p, q) and $(p \pm 1, q)$ is C_{dd} , whereas the interaction between bosons at lattice sites (p, q) and $(p, q \pm 1)$ is $U_{dd}(\theta) = C_{dd}(1 - 3\sin^2 \theta)$.

where U and $C_{dd} \propto d^2/a^3$ are the strengths of the on-site and dipolar interactions, respectively. Here, d is the magnitude of the induced dipole moment, and α_{ij} is the angle between the polarization axis and the vector $(\vec{r}_j - \vec{r}_i)$. In units of a the position vectors of the lattices $\vec{r}_i \equiv (p\hat{e}_x + q\hat{e}_y)$ and $\vec{r}_j \equiv (p'\hat{e}_x + q'\hat{e}_y)$.

In our study, for simplicity, we limit the dipolar interaction to NN sites. Then

$$\hat{H}_I = \sum_i \frac{U}{2} \hat{n}_i (\hat{n}_i - 1) + \frac{C_{dd}}{2} \sum_{\langle ij \rangle} \hat{n}_i \hat{n}_j (1 - 3\cos^2 \alpha_{ij}). \quad (3)$$

This minimal model is apt for studying the quantum phases of dipolar bosons emerging from the anisotropic nature of the dipolar interaction. The anisotropy in the NN interaction arises due to the canting of the polarization axis, which makes an angle θ and ϕ with the positive z and x axes, respectively. The NN interaction is isotropic when $\theta = 0^\circ$, that is, the dipoles are aligned along the z axis, and for any value of θ when $\phi = 45^\circ$. For all other combinations of θ and ϕ the NN interaction is anisotropic. The anisotropy for a given nonzero θ is maximum when $\phi = 0^\circ$ or 90° , that is, the dipoles are polarized in the xz or yz planes, respectively. In our study, we consider the dipoles to be polarized in the yz plane as illustrated in Fig. 1. So, the model can accommodate all possible phases of the system stemming from the anisotropic NN interaction. Then by definition θ is the tilt angle. With this choice, α_{ij} changes as a function of θ , which can be varied by changing the orientation of the applied magnetic field. Then the NN interaction along the x axis is always repulsive, constant, and independent of θ , whereas along the y axis the NN interaction is $U_{dd}(\theta) = C_{dd}(1 - 3\sin^2 \theta)$. It varies from C_{dd} to $-2C_{dd}$ as θ is tuned from 0° to 90° . And the zero of $U_{dd}(\theta)$ occurs when $\theta = \theta_M = \sin^{-1}(1/\sqrt{3}) \approx 35.3^\circ$. This angle is referred to as the magic angle [59] and at this tilt angle the interaction arising from the dipolar interaction is

absent along the y axis. Thus, the interaction along the y axis is repulsive when $\theta < 35.3^\circ$ and attractive when $\theta > 35.3^\circ$.

III. THEORETICAL METHODS

A. Gutzwiller mean-field theory

To solve the model, we consider the site decoupled mean-field approximation [1,60–64]. For this, the bosonic annihilation operator of site (p, q) , $\hat{b}_{p,q}$, is decomposed to an MF $\phi_{p,q}$ and fluctuation operator $\delta\hat{b}_{p,q}$ as $\hat{b}_{p,q} = \langle\hat{b}_{p,q}\rangle + \delta\hat{b}_{p,q} = \phi_{p,q} + \delta\hat{b}_{p,q}$. A similar decomposition is applied to $\hat{b}_{p,q}^\dagger$ and $\hat{n}_{p,q}$. Henceforth, we adopt the explicit notation (p, q) to denote a lattice site in two dimensions. To obtain the MF Hamiltonian, we use the decomposed operators in \hat{H} and neglect the terms which are quadratic in fluctuation operators. Then the MF Hamiltonian of the system is

$$\begin{aligned} \hat{H}_{\text{MF}} = \sum_{p,q} & \left\{ -J[(\hat{b}_{p+1,q}^\dagger \phi_{p,q} + \phi_{p+1,q}^* \hat{b}_{p,q} - \phi_{p+1,q}^* \phi_{p,q}) \right. \\ & + (\hat{b}_{p,q+1}^\dagger \phi_{p,q} + \phi_{p,q+1}^* \hat{b}_{p,q} \\ & - \phi_{p,q+1}^* \phi_{p,q}) + \text{H.c.}] - \mu \hat{n}_{p,q} \\ & + \frac{U}{2} \hat{n}_{p,q} (\hat{n}_{p,q} - 1) + \frac{C_{\text{dd}}}{2} [(\hat{n}_{p+1,q} \langle\hat{n}_{p,q}\rangle + \langle\hat{n}_{p+1,q}\rangle \hat{n}_{p,q} \\ & - \langle\hat{n}_{p+1,q}\rangle \langle\hat{n}_{p,q}\rangle) + (\hat{n}_{p-1,q} \langle\hat{n}_{p,q}\rangle + \langle\hat{n}_{p-1,q}\rangle \hat{n}_{p,q} \\ & - \langle\hat{n}_{p-1,q}\rangle \langle\hat{n}_{p,q}\rangle)] + \frac{U_{\text{dd}}(\theta)}{2} [(\hat{n}_{p,q+1} \langle\hat{n}_{p,q}\rangle \\ & + \langle\hat{n}_{p,q+1}\rangle \hat{n}_{p,q} - \langle\hat{n}_{p,q+1}\rangle \langle\hat{n}_{p,q}\rangle) \\ & \left. + (\hat{n}_{p,q-1} \langle\hat{n}_{p,q}\rangle + \langle\hat{n}_{p,q-1}\rangle \hat{n}_{p,q} - \langle\hat{n}_{p,q-1}\rangle \langle\hat{n}_{p,q}\rangle)] \right\}. \quad (4) \end{aligned}$$

This can be written in terms of single-site Hamiltonians as

$$\hat{H}_{\text{MF}} = \sum_{p,q} \hat{h}_{p,q}, \quad (5)$$

where $\hat{h}_{p,q}$ is the single-site Hamiltonian of site (p, q) , which can be expressed as

$$\begin{aligned} \hat{h}_{p,q} = & -J[(\phi_{p+1,q}^* \hat{b}_{p,q} + \phi_{p,q+1}^* \hat{b}_{p,q} + \phi_{p-1,q}^* \hat{b}_{p,q} \\ & + \phi_{p,q-1}^* \hat{b}_{p,q}) + \text{H.c.}] - \mu \hat{n}_{p,q} + \frac{U}{2} \hat{n}_{p,q} (\hat{n}_{p,q} - 1) \\ & + \frac{C_{\text{dd}}}{2} \hat{n}_{p,q} (\langle\hat{n}_{p+1,q}\rangle + \langle\hat{n}_{p-1,q}\rangle) \\ & + \frac{U_{\text{dd}}(\theta)}{2} \hat{n}_{p,q} (\langle\hat{n}_{p,q+1}\rangle + \langle\hat{n}_{p,q-1}\rangle), \quad (6) \end{aligned}$$

where we have dropped the pure MF terms. These terms shift the ground-state energy and play no role in determining the ground state or the phase diagrams of the system. We can solve the model by diagonalizing the single-site Hamiltonians coupled through the mean-field $\phi_{p,q}$ self-consistently. To obtain the ground state of the system, we consider the site-dependent Gutzwiller (GW) ansatz

$$|\Psi_{\text{GW}}\rangle = \prod_{p,q} |\psi_{p,q}\rangle = \prod_{p,q} \sum_{n=0}^{(N_b-1)} c_n^{(p,q)} |n\rangle_{p,q}, \quad (7)$$

where $\{|n\rangle_{p,q}\}$ are the occupation number basis states at site (p, q) , N_b is the total number of local Fock states used in the computation, and $c_n^{(p,q)}$ are complex coefficients of the ground state $|\Psi_{\text{GW}}\rangle$. The normalization of $|\Psi_{\text{GW}}\rangle$ is ensured by considering the sitewise normalization condition

$$\langle\psi_{p,q}|\psi_{p,q}\rangle = \sum_{n=0}^{(N_b-1)} |c_n^{(p,q)}|^2 = 1. \quad (8)$$

Then the mean-field or superfluid order parameter $\phi_{p,q}$ and the average occupancy $n_{p,q}$ at the lattice site (p, q) are

$$\begin{aligned} \phi_{p,q} = \langle\Psi_{\text{GW}}|\hat{b}_{p,q}|\Psi_{\text{GW}}\rangle & = \sum_{n=1}^{(N_b-1)} \sqrt{n} c_{n-1}^{(p,q)*} c_n^{(p,q)}, \\ n_{p,q} = \langle\Psi_{\text{GW}}|\hat{n}_{p,q}|\Psi_{\text{GW}}\rangle & = \sum_{n=0}^{(N_b-1)} n |c_n^{(p,q)}|^2. \quad (9) \end{aligned}$$

As the name indicates, $\phi_{p,q}$ is a nonzero quantity in the SF phase, and from the definition, it is an indicator of the number fluctuation. Hence, it is a measure of the long-range phase coherence in the system. In other words, the SF phase has off-diagonal long-range order (ODLRO). Another relevant parameter of a quantum phase is the average occupancy per lattice site ρ . For a system size of $K \times L$

$$\rho = \frac{1}{K \times L} \sum_{p=1, q=1}^{K, L} n_{p,q}. \quad (10)$$

In the present work we study quantum phases in the hard-core as well as the soft-core regimes; in these regimes $\rho \leq 1$ and $\rho \geq 1$, respectively.

B. Quantum phases and their characterization

In the absence of a dipolar interaction, depending on J/U there are two ground-state quantum phases of the system: the superfluid and Mott insulator phases. The key distinction between these two phases is that $\phi_{p,q}$, as mentioned earlier, is finite in the SF phase. But it is 0 in the MI phase. In a homogeneous lattice system, the density distribution of these two phases is uniform. However, this translational symmetry can be spontaneously broken with a long-range dipole-dipole interaction. This leads to the emergence of quantum phases which have periodic density modulations, such as the density wave and supersolid. In other words, the system can exhibit diagonal order. Among the two phases the SS phase, in addition to the diagonal order, has ODLRO. Therefore, the SS phase has nonzero $\phi_{p,q}$, and $n_{p,q}$ has a periodic structure. On the other hand, for the DW phase, as in the MI phase, $\phi_{p,q}$ is 0 and $n_{p,q}$ is an integer. But unlike the MI phase, $n_{p,q}$ in the DW show a spatial pattern. To characterize the diagonal order in the DW and SS phases, we compute the static structure factor,

$$S(\vec{k}) = \frac{1}{N^2} \sum_{i,j} e^{i\vec{k} \cdot (\vec{r}_i - \vec{r}_j)} \langle\hat{n}_i \hat{n}_j\rangle, \quad (11)$$

where $\vec{k} \equiv (k_x, k_y) \equiv (k_x \hat{e}_x + k_y \hat{e}_y)$ is the reciprocal lattice vector (measured in units of $1/a$), and N is the total number of bosons in the system. In the present study, depending on the

TABLE I. Characteristics of different quantum phases of the considered system.

| Quantum phase | $n_{p,q}$ | $\phi_{p,q}$ | $S(\pi, \pi)$ | $S(\pi, 0)$ |
|----------------------------------|-----------|--------------|---------------|-------------|
| Superfluid (SF) | Real | $\neq 0$ | 0 | 0 |
| Mott insulator (MI) | Integer | 0 | 0 | 0 |
| Checkerboard supersolid (CBSS) | Real | $\neq 0$ | $\neq 0$ | 0 |
| Striped supersolid (SSS) | Real | $\neq 0$ | 0 | $\neq 0$ |
| Emulsion supersolid | Real | $\neq 0$ | $\neq 0$ | $\neq 0$ |
| Checkerboard density wave (CBDW) | Integer | 0 | $\neq 0$ | 0 |
| Striped density wave (SDW) | Integer | 0 | 0 | $\neq 0$ |
| Emulsion density wave | Integer | 0 | $\neq 0$ | $\neq 0$ |

tilt angle θ , the system has $n_{p,q}$ which is either checkerboard or striped. The checkerboard order breaks the translational symmetry along both the x and the y directions and is characterized by a finite value of $S(\vec{k})$ at the reciprocal lattice site $\vec{k} = (\pi, \pi)$. In the phases having a striped pattern, the translational symmetry is broken only along the x direction. And $S(\vec{k})$ is nonzero only for $\vec{k} = (\pi, 0)$. Thus, the structure factors $S(\pi, \pi)$ and $S(\pi, 0)$ can be used to characterize the CB and striped phases. Like the MI phase, the DW phase is an incompressible phase of the system, whereas in the SF and SS phases, the system is compressible. Table I summarizes the distinct characteristics of the different possible phases of the considered system. It is important to note that the system can harbor a multitude of distinct structured states when the range of the dipolar interaction is considered beyond NNs [52,65]. Many of these states are nearly degenerate metastable states which compete with the ground state.

To illustrate the density distribution in the structured phases, the density distributions in the CBDW (1,0), SDW (1,0), and emulsion DW (1,0) are shown in Fig. 2. There the integer pair (n_1, n_2) denotes the occupancies of two consecutive lattice sites along the x direction. As expected, in Fig. 2(a) the density modulation of the CBDW (1,0) phase is along both directions. And in Fig. 2(b) for the SDW (1,0) phase the density modulation is along the x axis. The emulsion state, as shown in Fig. 2(c), has regions with both types of

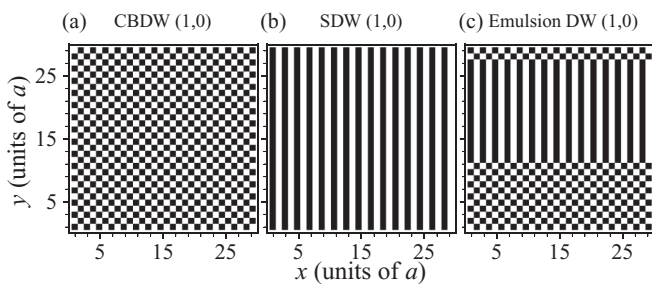


FIG. 2. Density pattern of the system in distinct density-wave phases. Black squares represent lattice sites which are vacant, and white squares denote singly occupied lattice sites. The states are illustrated for fixed $\mu/J = 15$ and $C_{dd}/U = 0.8$. CBDW (1,0) and SDW (1,0) states are obtained for $J/U = 0.033$ at $\theta = 0^\circ$ and 37° , respectively. The emulsion state is obtained for $J/U = 0.035$ at $\theta = 31.5^\circ$.

density modulations. These emulsion states are an admixture of ground and excited states having checkerboard or striped order, and they appear near the parameter domain of the checkerboard-to-striped phase transition. In this regime, states with checkerboard and striped patterns are nearly degenerate. So, regions with checkerboard and striped patterns can coexist in the emulsion states, which is evident upon visual inspection of the density distribution shown in Fig. 2(c). The size of these regions depends on the system size and initial guess states considered in our computations. In general, the region corresponding to the actual ground state is like a background, with the excited state occurring as patches. The simultaneous existence of the two orders is also reflected in the nonzero values of the structure factors $S(\pi, \pi)$ and $S(\pi, 0)$. The density distributions of the checkerboard, striped, and emulsion SS states are similar to the density pattern in Fig. 2, except that $n_{p,q}$ are real, whereas it is integer in the DW phases. In addition, the SS phases have $\phi_{p,q}$ with patterns similar to $n_{p,q}$. But $\phi_{p,q}$ is uniform in the SF phase, which is reminiscent of the uniform density distribution in this phase.

C. Phase boundaries from mean-field decoupling theory

To gain additional insights into the phase transitions between compressible and incompressible phases we calculate the phase boundaries analytically using the mean-field decoupling theory [66,67]. A similar analysis can be done using other methods like strong-coupling expansion [67–69] or the random phase approximation [70]. For this we use the decoupling scheme, described earlier, $\hat{b}_{p,q} = \phi_{p,q} + \delta \hat{b}_{p,q}$, $\hat{b}_{p,q}^\dagger = \phi_{p,q}^* + \delta \hat{b}_{p,q}^\dagger$, and $\hat{n}_{p,q} = n_{p,q} + \delta \hat{n}_{p,q}$. Here, the SF order parameter, $\phi_{p,q}$, is nonzero in the SF and SS phases but 0 in the MI and DW phases. We assume that the phase transition between a compressible ($\phi_{p,q} \neq 0$) and an incompressible ($\phi_{p,q} = 0$) phase is continuous. Then the energy can be defined as a smooth function of $\phi_{p,q}$ across the phase boundary and the perturbation analysis is applicable. With this consideration, the phase boundary between a compressible and an incompressible phase is marked by a vanishing SF order parameter $\phi_{p,q} \rightarrow 0^+$. In addition, the MI and DW phases correspond to integer occupancies per lattice site and are the exact eigenstates of the interaction and chemical potential part of the MF Hamiltonian in Eq. (4). Thus, the hopping term in the Hamiltonian can be considered as a perturbation with $\phi_{p,q}$ as the perturbation parameter. We can then perform a perturbative analysis (details are given in Appendix A) to obtain the order parameter from the first-order wave function as

$$\phi_{p,q} = J \bar{\phi}_{p,q} \left[\frac{n_{p,q} + 1}{U n_{p,q} - \tilde{\mu}_{p,q}} - \frac{n_{p,q}}{U (n_{p,q} - 1) - \tilde{\mu}_{p,q}} \right], \quad (12)$$

where $\tilde{\mu}_{p,q} = \mu - V_{p,q}^{\text{dip}}$ and

$$\bar{\phi}_{p,q} = (\phi_{p+1,q} + \phi_{p-1,q} + \phi_{p,q+1} + \phi_{p,q-1}),$$

$$V_{p,q}^{\text{dip}} = \frac{C_{dd}}{2} (n_{p+1,q} + n_{p-1,q}) + \frac{U_{dd}(\theta)}{2} (n_{p,q+1} + n_{p,q-1}).$$

A similar equation is obtained from the Landau procedure for continuous phase transition. In this case the energy functional

defined as a function of $\phi_{p,q}$ is minimized [53,71]. In the MI phase, the system has integer commensurate filling, say n_0 , and in the SF phase it has a uniform SF order parameter φ_0 . With these considerations,

$$\begin{aligned}\bar{\phi}_{p,q} &\equiv \bar{\phi} = 4\varphi_0, \\ \tilde{\mu}_{p,q} &\equiv \tilde{\mu} = \mu - [C_{dd} + U_{dd}(\theta)]n_0.\end{aligned}$$

Since in the SF phase $\varphi_0 \rightarrow 0^+$ near the phase boundary, then from Eq. (12) the MI-SF phase boundary can be calculated from

$$\frac{1}{4J} = \left[\frac{n_0 + 1}{Un_0 - \tilde{\mu}} - \frac{n_0}{U(n_0 - 1) - \tilde{\mu}} \right]. \quad (13)$$

The solution of the above equation defines the MI-SF boundary in the μ - J plane corresponding to the MI lobe with n_0 filling.

To describe the phase transition from the DW to the SS phase, we consider a two-sublattice description of the phases. That is, dipolar-interaction-induced solid order or spatially periodic modulation can be considered as if the system has two sublattices, A and B . Each sublattice has different occupancies n_A and n_B as well as two order parameters, φ_A and φ_B . In the checkerboard order the periodic modulation is along both the x and the y directions with a period of $2a$, whereas in the striped order the modulation is along one of the directions. So, to obtain the phase boundary between the SDW and the SSS phases from Eq. (12), we consider a striped sublattice structure. Therefore, we define $\bar{\phi}_{p,q} = 2(\varphi_A + \varphi_B)$, $\tilde{\mu}_A = \mu - [C_{dd}n_B + U_{dd}(\theta)n_A]$ for the $(p, q) \in A$ sublattice and $\bar{\phi}_{p,q} = 2(\varphi_A + \varphi_B)$, $\tilde{\mu}_B = \mu - [C_{dd}n_A + U_{dd}(\theta)n_B]$ for the $(p, q) \in B$ sublattice. This leads to two coupled equations for φ_A and φ_B :

$$\varphi_A = 2(\varphi_A + \varphi_B)J \left[\frac{n_A + 1}{Un_A - \tilde{\mu}_A} - \frac{n_A}{U(n_A - 1) - \tilde{\mu}_A} \right], \quad (14a)$$

$$\varphi_B = 2(\varphi_A + \varphi_B)J \left[\frac{n_B + 1}{Un_B - \tilde{\mu}_B} - \frac{n_B}{U(n_B - 1) - \tilde{\mu}_B} \right]. \quad (14b)$$

We solve these two equations simultaneously. In the SSS phase $\{\varphi_A, \varphi_B\} \rightarrow 0^+$ across the SDW-SSS phase boundary. Then the SDW-SSS phase boundary is obtained as the solution of

$$\begin{aligned}\frac{1}{2J} &= \left[\frac{n_A + 1}{Un_A - \tilde{\mu}_A} - \frac{n_A}{U(n_A - 1) - \tilde{\mu}_A} \right] \\ &+ \left[\frac{n_B + 1}{Un_B - \tilde{\mu}_B} - \frac{n_B}{U(n_B - 1) - \tilde{\mu}_B} \right]. \quad (15)\end{aligned}$$

Following similar reasoning, the CBDW-CBSS phase boundary is obtained as the solution of

$$\begin{aligned}\frac{1}{16J^2} &= \left[\frac{n_A + 1}{Un_A - \tilde{\mu}_A} - \frac{n_A}{U(n_A - 1) - \tilde{\mu}_A} \right] \\ &\times \left[\frac{n_B + 1}{Un_B - \tilde{\mu}_B} - \frac{n_B}{U(n_B - 1) - \tilde{\mu}_B} \right]. \quad (16)\end{aligned}$$

For $\theta = 0^\circ$, this becomes identical to the phase boundary in two dimensions reported by Iskin [53]. The detailed steps

of derivations to obtain the above equation are discussed in Appendix B.

It is to be mentioned here that close to θ_M , the system undergoes a checkerboard-stripped transition. So, in this regime the system can exhibit both orders simultaneously, leading to emulsion DW states. The parameter domains of such emulsion DW states can be identified as the regions where Eqs. (15) and (16) are both applicable.

IV. NUMERICAL METHODS

To obtain the equilibrium phase diagrams of the system, we diagonalize the single-site Hamiltonian in Eq. (6) [62,63]. For this, we consider a guess solution of the ground state $|\Psi_{GW}\rangle$ to compute the initial values of $\phi_{p,q}$ and $\langle \hat{n}_{p,q} \rangle$. In general we choose the initial guess state $|\psi_{p,q}\rangle$ to be the same for all lattice sites (p, q) and consider $c_n^{(p,q)} = 1/\sqrt{N_b}$. This corresponds to the uniform distribution of $n_{p,q}$ and $\phi_{p,q}$. We then use the initial values of $n_{p,q}$ and $\phi_{p,q}$ in Eq. (6) and diagonalize it to obtain a new ground state, $|\psi_{p,q}\rangle$. Using this new state we update $|\Psi_{GW}\rangle$ and then compute the corresponding $\phi_{p,q}$ and $\langle \hat{n}_{p,q} \rangle$. We then repeat the same for the next lattice site. This is repeated till all the lattices sites are covered. One such step constitutes an iteration, and the iteration is repeated till $\phi_{p,q}$ and $\langle \hat{n}_{p,q} \rangle$ converge. Around the phase boundary the convergence is slow and this is remedied by considering a larger number of iterations. To model a uniform infinite-sized lattice, we perform the above procedure on the surface of a torus by considering periodic boundary conditions along the x and y directions of the finite-sized lattice system. In general, we have considered a 12×12 lattice system and $N_b = 20$ to obtain the phase diagrams. System size and initial guess state dependence of the phase boundary occurs when there is an intervening region of emulsion states between two phases. For these special cases, we supplement the results for a 12×12 lattice with the results obtained for 20×20 and 30×30 lattice systems. And we corroborate the stability of the obtained ground states with respect to different initial guess states having an inhomogeneous distribution in $n_{p,q}$ and $\phi_{p,q}$. We have considered initial guess states which have checkerboard, horizontal and vertical striped, and random density patterns satisfying the normalization condition in Eq. (8).

V. RESULTS AND DISCUSSION

The model Hamiltonian considered has five independent parameters, namely, J , U , μ , C_{dd} , and θ . To examine the phase diagram of the system in detail we scale the Hamiltonian with respect to J and set $\mu/J = 15$. This reduces the number of independent parameters to three: U/J , C_{dd}/J , and θ . For better description, we obtain the phase diagrams in the J/U - C_{dd}/U plane for different values of θ . This choice is suitable to probe the interplay between on-site and dipolar interactions in determining the distinct phases of the system.

A. J/U - C_{dd}/U phase diagrams

J/U - C_{dd}/U phase diagrams for different values of θ are shown in Fig. 3. In the figure, solid lines correspond to phase

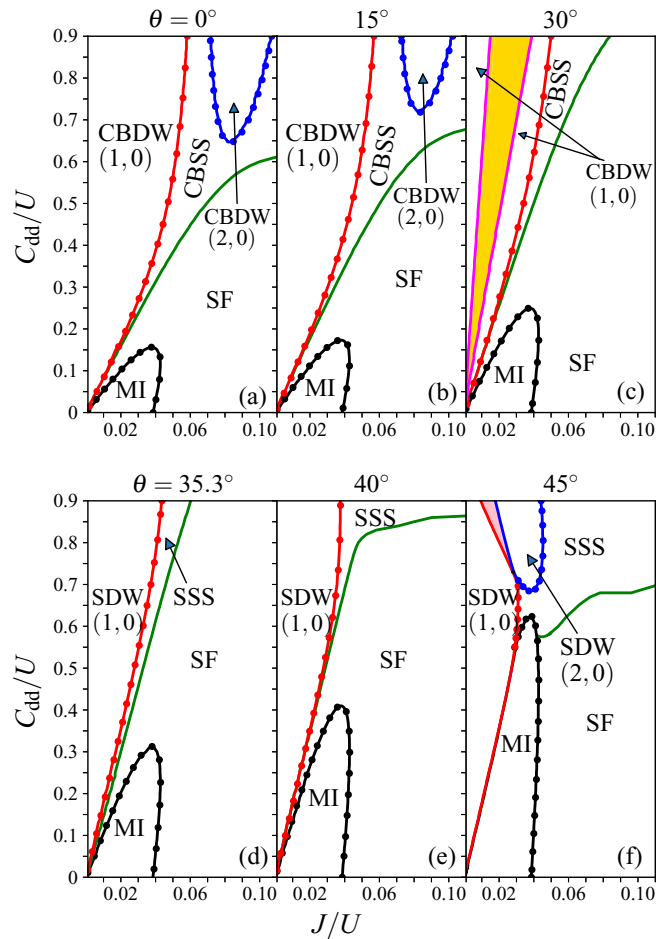


FIG. 3. Phase diagrams in the J/U - C_{dd}/U plane for different values of the tilt angle θ . The phase diagrams are obtained for $\mu/J = 15$. Solid phase boundaries are obtained from the self-consistent numerical diagonalization of the mean-field Hamiltonian of the system, whereas filled circles represent the phase boundaries between an incompressible and a compressible phase of the system, which are obtained analytically considering perturbation analysis of the mean-field decoupling theory. In (c), the parameter region for the emulsion DW (1,0) state is shaded gold. In the emulsion state, the system simultaneously exhibits both orders, checkerboard and striped. The parameter region shaded pink in (f) represents the emulsion of SDW (1,0) and SDW (2,0) phases.

boundaries obtained from the Gutzwiller MF theory. Filled circles represent phase boundaries between an incompressible and a compressible phase, which are calculated from the MF decoupling theory. In the figure, it is evident that the mean-field decoupling theory, when applicable, gives results which are in good agreement with the Gutzwiller mean-field theory. For the parameters considered we obtain an MI phase with unit filling. The MI-SF phase boundary is obtained by solving Eq. (13) with $n_0 = 1$. The SSS-SDW phase boundaries are calculated by solving Eq. (15) with $n_A = 1$ and $n_B = 0$ for the SDW (1,0)-SSS boundary and $n_A = 2$ and $n_B = 0$ for the SDW (2,0)-SSS boundary. Similarly, the CBSS-CBDW phase boundaries are calculated by solving Eq. (16) with $n_A = 1$ and $n_B = 0$ for the CBDW (1,0)-CBSS boundary and $n_A = 2$ and $n_B = 0$ for the CBDW (2,0)-CBSS boundary.

1. $\theta = 0^\circ, 15^\circ$, and 30°

The phase diagrams for $\theta = 0^\circ, 15^\circ$, and 30° are shown in Figs. 3(a), 3(b) and 3(c). These are representative cases for a tilt angle lower than the magic angle, that is, $\theta < 35.3^\circ$. For these θ , U_{dd} is repulsive along both the x and the y directions. The interaction is isotropic when $\theta = 0^\circ$, and along the y axis the interaction strength decreases with an increase in θ . For lower values of C_{dd}/U the system is in the DW or SF or MI phase for all values of θ . Of these, the MI and SF phases do not have diagonal order. But for higher values of C_{dd}/U the system favors phases with diagonal order. And we also get the CBSS phase in which the system exhibits ODLRO in addition to diagonal order. In addition, there are domains in the phase diagram where CBDW phases with different filling exist.

In the DW phases ODLRO is absent and the system has only diagonal order. By comparing the phase diagrams shown in Figs. 3(a) to 3(c), we can infer that the domain with checkerboard order diminishes with an increase in θ . This is due to the decrease in U_{dd} , which increases the anisotropy of the dipolar interaction, and checkerboard order becomes energetically unfavorable. At $\theta = 30^\circ$, as shown in Fig. 3(c), we obtain metastable emulsion DW states. The parameter domain of these states is shaded gold. In an emulsion state, the checkerboard and striped orders coexist. The emergence of the emulsion states at this tilt angle implies that U_{dd} is weak and cannot support checkerboard order. The system has entered the parameter domain where the striped order has a lower energy. Indeed, at larger θ we obtain phases with striped order. In addition, an important aspect of the phase diagram at $\theta = 30^\circ$ is the absence of the DW (2,0) phase. It is to be mentioned here that the phase diagram for $\theta = 0^\circ$, shown in Fig. 3(a), is consistent with the results reported in our previous work [64]. In our previous work, we explored the phase diagram of the extended BHM model in the J/U - μ/U plane. And, thus, parts of the phase diagram for specific values of C_{dd}/U and μ/J in Fig. 3(a) correspond to horizontal cuts of the phase diagram reported in Ref. [64].

2. $\theta = 35.3^\circ$ and 40°

At the magic angle, that is, $\theta = \theta_M \approx 35.3^\circ$, as mentioned earlier, the dipolar interaction along the y axis vanishes. But the interaction along the x axis remains positive and unchanged. Energetically, this favors striped order for phases with diagonal order. And as shown in Fig. 3(d), the phase diagram supports SSS and SDW phases. For $\theta > \theta_M$, the dipolar interaction along the y axis is attractive. This further enhances the striped phases, and this is discernible from the phase diagram at $\theta = 40^\circ$ shown in Fig. 3(e). In this case, the SSS phase extends up to $J/U \approx 0.2$ for $C_{dd}/U \approx 0.9$.

3. $\theta = 45^\circ$

At higher θ , new striped phases emerge in the phase diagram, and as an example we examine the phase diagram at $\theta = 45^\circ$. As shown in Fig. 3(f), the SDW (2,0) phase is present in the system when $\theta = 45^\circ$. However, at lower θ , the stronger attractive interaction along the y axis results in instability of the system and ultimately leads to density collapse. The phase diagram at $\theta = 45^\circ$ shows two distinct signatures of the onset of instability: first, the mixing of different phases, SDW

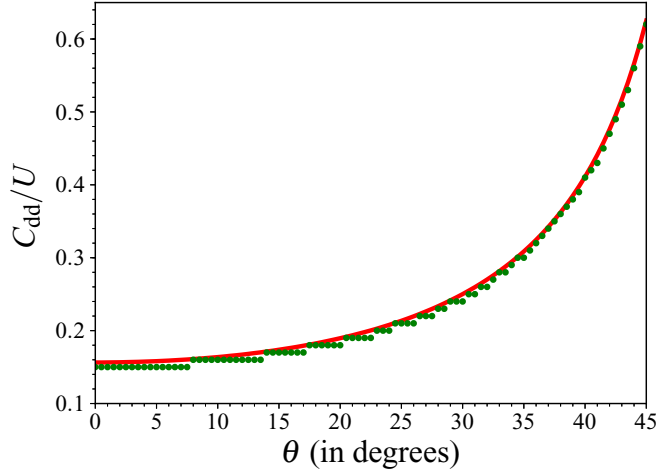


FIG. 4. C_{dd}/U value of the tip of the MI lobe as the tilt angle θ is changed. Filled green circles are obtained from Gutzwiller mean-field theory and the solid red line is obtained from Eq. (13).

(1,0) and SDW (2,0), in the domain shaded pink and, second, the merging of different phases, MI, SF, SSS, and SDW. In contrast, at lower θ the incompressible phases are separated by an intervening compressible phase. It must be mentioned here that merging of incompressible phases is also discussed in previous works on the 2D BHM with a three-body attractive interaction [72,73]. The presence of emulsion states indicates that the phase transition between SDW (1,0) and SDW (2,0) phases is not second-order. A detailed analysis is essential to understand whether the phase transition is first-order or a microemulsion phase intervenes the transition [74].

In the phase diagram there is a triple point of MI, SDW (1,0), and SSS phases at approximately (0.027,0.5). Starting from the triple point there is a sharp phase boundary between the MI phase with unit filling and the SDW (1,0) phase in the range $0.38 \leq C_{dd}/U \leq 0.50$ and $0.021 \lesssim J/U \lesssim 0.027$. Either this phase boundary could be a first-order phase transition or a thin region of metastable emulsion of the two phases could exist which is not detectable with the present method. However, for $J/U < 0.021$ and $C_{dd}/U < 0.38$, we do obtain a very narrow region of the emulsion states separating these two phases. In this context, it is important to mention that a phase transition between MI and DW phases has been observed in a quantum degenerate gas of ^{87}Rb atoms in a 3D optical lattice immersed in a cavity [75]. The signature of metastability across the phase transition has been identified and attributed to the competition between short-range on-site and long-range cavity-mediated interactions.

4. MI lobe enhancement

One feature of the MI lobe discernible from the phase diagrams in Fig. 3 is its enhancement along the C_{dd}/U axis with increasing θ . To illustrate this, the θ dependence of the MI lobe tip, in terms of C_{dd}/U , is shown in Fig. 4. To analyze this consider Eq. (13), which defines the MI-SF boundary in the mean-field decoupling theory, and rewrite it as

$$\frac{U}{4J} = \left[\frac{n_0 + 1}{n_0 - \tilde{\mu}/U} - \frac{n_0}{(n_0 - 1) - \tilde{\mu}/U} \right]. \quad (17)$$

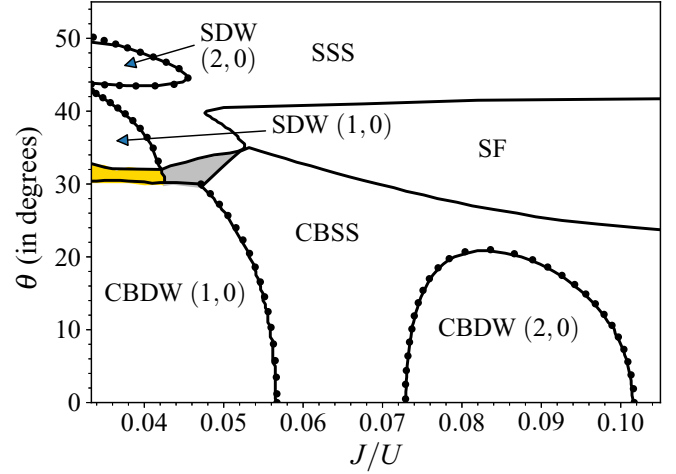


FIG. 5. Phase diagram in the J/U - θ plane for $C_{dd}/U = 0.8$ and $\mu/J = 15$. Solid phase boundaries are obtained from the numerical computation of the Gutzwiller mean-field theory. Filled circles mark the phase boundaries between an incompressible and a compressible phase, which are calculated analytically by performing perturbation analysis of the mean-field decoupling theory. Parameter domains shaded silver and gold represent emulsion SS and emulsion DW (1,0) states, respectively. In these emulsion states, checkerboard and striped order coexist in the system.

In the absence of the dipolar interaction ($C_{dd} = 0$) $\tilde{\mu} = \mu$ and we obtain the MI-SF boundary of the BHM. However, the dipolar interaction reduces the effective chemical potential to $\tilde{\mu} = \mu - C_{dd}(2 - 3 \sin^2 \theta)$. At $\theta = 0^\circ$, $\tilde{\mu}$ has the smallest value, $\tilde{\mu}_{\min} = \mu - 2C_{dd}$, and this can be considered the value of $\tilde{\mu}$ that defines the MI-SF boundary. But when $\theta > 0^\circ$ the prefactor $(2 - 3 \sin^2 \theta)$ decreases, and hence, to maintain the same value of $\tilde{\mu}$ the strength of the dipolar interaction C_{dd} has to increase. Thus, there is an enhancement of the MI lobe along the C_{dd}/U axis. As the degree of enhancement depends on the prefactor with $\sin^2 \theta$, the trend noticeable in Fig. 4 is indicative of this dependence. This is consistent with the experimental finding in [23], where the on-site repulsive dipolar interaction is observed to favor the MI phase due to stronger pinning of the lattice bosons.

B. Phase diagrams in the J/U - θ plane

From the phase diagrams in Fig. 3, it is evident that the phase structure is richer with a stronger dipolar interaction (large C_{dd}/U). Most importantly, the checkerboard order of the system transforms into striped order below a certain value of θ . This is an example of the structural phase transition. To examine the phases of the system as a function of θ we examine the phase diagram in the J/U - θ plane for fixed values of C_{dd}/U and μ/J . And as an example the phase diagram in the case of $C_{dd}/U = 0.8$ and $\mu/J = 15$ is shown in Fig. 5. Consistent with the phase diagrams in Fig. 3, checkerboard and striped orders are preferred for $\theta \lesssim 25^\circ$ and $\theta \gtrsim 35^\circ$, respectively. For $25^\circ \lesssim \theta \lesssim 35^\circ$ emulsion states are preferred in the strongly interacting domain. The parameter regions of the emulsion DW and emulsion SS states are shaded gold and silver, respectively. However, in the weakly interacting domain, $J/U \gtrsim 0.053$, the SF phase is the intervening

phase between checkerboard and striped supersolids. These are in good agreement with the previous findings on the phase transition between CBDW (1,0) and SDW (1,0) in the hard-core limit of the model [58]. The intervening emulsion and SF phases imply that there is no sharp phase transition between the two structured phases. And, also, it cannot be a second-order phase transition in the strongly interacting domain, $J/U \lesssim 0.053$. In this domain, the phase transition can be either a first-order or a ‘‘Spivak-Kivelson’’-type phase transition in which a microemulsion phase intervenes between two ordered phases [74]. The fact that the checkerboard order disappears at θ smaller than the magic angle implies that it is a delicate phase. It is unstable against large anisotropy of the interaction potential. At larger θ an attractive NN interaction along the y direction dominates, which renders the system unstable. The total NN interaction energy becomes attractive for $\theta > \sin^{-1}(\sqrt{2/3}) \approx 54.7^\circ$. In our computations, however, the collapse arising from an attractive interaction occurs when $\theta \gtrsim 55^\circ$. It is important to mention that the competition between the attractive NN interaction along the y direction and the repulsive on-site plus NN interaction along the x direction determines the stability against collapse of the system. Using magnetic Feshbach resonances, the on-site interaction strength U can be tuned in atomic dipolar gases [22,76–80]. But for the stability of the system, U is required always to be positive. An attractive on-site interaction, however small, makes the system unstable and it collapses. However, stable phases can be obtained in a three-body hard-core constraint system with an attractive on-site interaction [81,82].

An important observation, manifest in Fig. 5, is the parameter domain of the CBDW (2,0) and SDW (2,0) phases. The former occurs in the domain of large J/U and small θ . The latter, on the other hand, occurs in the domain with small J/U and large θ . This is, however, due to the choice of C_{dd}/U and μ/J . For a different choice of these two parameters, there could be an intervening region of emulsion states for the transition between these two structured phases.

VI. CONCLUSIONS

In conclusion, we have explored the rich phase structure of soft core dipolar bosons in a 2D optical lattice as a function of the tilt angle θ . A dipolar interaction in the soft-core regime induces the supersolid phase in this system and can withstand density-wave phases having unit or larger filling. The key point is that the variation of θ modifies the anisotropy of the dipolar interaction in the plane of the 2D square lattice. And this leads to the formation of two types of quantum phases with different diagonal orders: checkerboard and striped. Our results indicate that the quantum phase transition between these orders, namely, the checkerboard and striped orders, occurs through an intervening region of emulsion states. The striped order phases, both density-wave and supersolid phases, are preferred at high values of θ when the anisotropy is large. However, above the magic angle $\theta_M \approx 35.3^\circ$, as the interaction along the y axis becomes negative, a density instability manifests in the system. At $\theta = 45^\circ$, the system can undergo a quantum phase transition from one incompressible phase to another without passing through an intermediate compressible phase. We report such phase transitions between

the unit filling MI phase, (1,0) SDW, and (2,0) SDW phases. Our results can be experimentally examined since tilting the dipoles has become a standard tool to understand the physics of ultracold dipolar bosons and fermions [83–85].

ACKNOWLEDGMENTS

We thank R. Sachdeva and S. A. Silotri for valuable discussions. The results presented in the paper are based on computations using Vikram-100, the 100TFLOP HPC Cluster at Physical Research Laboratory, Ahmedabad, India. R.N. acknowledges funding from the Indo-French Centre for the Promotion of Advanced Research and UKIERI-UGC Thematic Partnership No. IND/CONT/G/16-17/73 UKIERI-UGC project. K.S. gratefully acknowledges the support of the National Science Centre, Poland, via project 2016/21/B/ST/2/01086.

APPENDIX A: PERTURBATIVE TREATMENT OF THE SF ORDER PARAMETER

We consider the hopping term in the single-site Hamiltonian as the perturbation and the interaction terms along with the chemical potential as the unperturbed Hamiltonian. Therefore, the energy of the ground state of the unperturbed Hamiltonian

$$E_{n_{p,q}}^0 = \frac{U}{2}n_{p,q}(n_{p,q} - 1) + \frac{C_{dd}}{2}n_{p,q}(n_{p+1,q} + n_{p-1,q}) + \frac{U_{dd}(\theta)}{2}n_{p,q}(n_{p,q+1} + n_{p,q-1}) - \mu n_{p,q}. \quad (\text{A1})$$

Then to first order in the SF order parameter, the perturbed ground state can be written as

$$|\psi_{p,q}\rangle = |n\rangle_{p,q} + \sum_{m \neq n} \frac{p,q \langle m | \hat{T}_{p,q} | n \rangle_{p,q}}{E_{n_{p,q}}^0 - E_{m_{p,q}}^0} |m\rangle_{p,q}, \quad (\text{A2})$$

where, considering the SF order parameter to be a real number,

$$\begin{aligned} \hat{T}_{p,q} &= -J(\phi_{p+1,q} + \phi_{p-1,q} + \phi_{p,q+1} + \phi_{p,q-1})(\hat{b}_{p,q} + \hat{b}_{p,q}^\dagger) \\ &= -J\bar{\phi}_{p,q}(\hat{b}_{p,q} + \hat{b}_{p,q}^\dagger). \end{aligned} \quad (\text{A3})$$

Therefore, using Eqs. (A1)–(A3) the ground state can be calculated as

$$|\psi_{p,q}\rangle = |n\rangle_{p,q} + J\bar{\phi}_{p,q} \left[\frac{\sqrt{n_{p,q} + 1}}{Un_{p,q} - \tilde{\mu}_{p,q}} |n_{p,q} + 1\rangle - \frac{\sqrt{n_{p,q}}}{U(n_{p,q} - 1) - \tilde{\mu}_{p,q}} |n_{p,q} - 1\rangle \right]. \quad (\text{A4})$$

From this state, we obtain the SF order parameter $\phi_{p,q}$ in the form mentioned in Eq. (12).

APPENDIX B: CBDW-CBSS PHASE BOUNDARY

To obtain the phase boundaries between the CBDW and the CBSS phases from Eq. (12), we consider the checkerboard sublattice structure. Then we define $\bar{\phi}_{p,q} = 4\phi_B$

and $\tilde{\mu}_A = \mu - [C_{dd} + U_{dd}(\theta)]n_B$ for the $(p, q) \in A$ sublattice and $\tilde{\phi}_{p,q} = 4\varphi_A$, $\tilde{\mu}_B = \mu - [C_{dd} + U_{dd}(\theta)]n_A$ for the $(p, q) \in B$ sublattice. This leads to two coupled equations:

$$\varphi_A = 4J\varphi_B \left[\frac{n_A + 1}{Un_A - \tilde{\mu}_A} - \frac{n_A}{U(n_A - 1) - \tilde{\mu}_A} \right], \quad (\text{B1a})$$

$$\varphi_B = 4J\varphi_A \left[\frac{n_B + 1}{Un_B - \tilde{\mu}_B} - \frac{n_B}{U(n_B - 1) - \tilde{\mu}_B} \right]. \quad (\text{B1b})$$

These two equations can be solved simultaneously. In the CBSS phase $\{\varphi_A, \varphi_B\} \rightarrow 0^+$ across the CBDW-CBSS phase boundary. Then the CBDW-CBSS phase boundary is obtained as in Eq. (16).

-
- [1] M. P. A. Fisher, P. B. Weichman, G. Grinstein, and D. S. Fisher, *Phys. Rev. B* **40**, 546 (1989).
- [2] D. Jaksch, C. Bruder, J. I. Cirac, C. W. Gardiner, and P. Zoller, *Phys. Rev. Lett.* **81**, 3108 (1998).
- [3] M. Greiner, O. Mandel, T. Esslinger, T. W. Hänsch, and I. Bloch, *Nature (London)* **415**, 39 (2002).
- [4] M. Greiner, O. Mandel, T. W. Hänsch, and I. Bloch, *Nature* **419**, 51 (2002).
- [5] J. Hubbard, *Proc. Roy. Soc. A* **276**, 238 (1963).
- [6] O. Penrose and L. Onsager, *Phys. Rev.* **104**, 576 (1956).
- [7] G. G. Batrouni and R. T. Scalettar, *Phys. Rev. Lett.* **84**, 1599 (2000).
- [8] E. Kim and M. H. W. Chan, *Nature* **427**, 225 (2004).
- [9] E. Kim and M. H. W. Chan, *Science* **305**, 1941 (2004).
- [10] K. Góral, L. Santos, and M. Lewenstein, *Phys. Rev. Lett.* **88**, 170406 (2002).
- [11] M. Boninsegni and N. Prokof'ev, *Phys. Rev. Lett.* **95**, 237204 (2005).
- [12] S. Yi, T. Li, and C. P. Sun, *Phys. Rev. Lett.* **98**, 260405 (2007).
- [13] I. Danshita and C. A. R. Sá de Melo, *Phys. Rev. Lett.* **103**, 225301 (2009).
- [14] T. Lahaye, C. Menotti, L. Santos, M. Lewenstein, and T. Pfau, *Rep. Prog. Phys.* **72**, 126401 (2009).
- [15] M. A. Baranov, M. Dalmonte, G. Pupillo, and P. Zoller, *Chem. Rev.* **112**, 5012 (2012).
- [16] H. P. Büchler and G. Blatter, *Phys. Rev. Lett.* **91**, 130404 (2003).
- [17] A. Griesmaier, J. Werner, S. Hensler, J. Stuhler, and T. Pfau, *Phys. Rev. Lett.* **94**, 160401 (2005).
- [18] J. Stuhler, A. Griesmaier, T. Koch, M. Fattori, T. Pfau, S. Giovanazzi, P. Pedri, and L. Santos, *Phys. Rev. Lett.* **95**, 150406 (2005).
- [19] T. Lahaye, T. Koch, B. Fröhlich, M. Fattori, J. Metz, A. Griesmaier, S. Giovanazzi, and T. Pfau, *Nature* **448**, 672 (2007).
- [20] M. Lu, N. Q. Burdick, S. H. Youn, and B. L. Lev, *Phys. Rev. Lett.* **107**, 190401 (2011).
- [21] Y. Tang, N. Q. Burdick, K. Baumann, and B. L. Lev, *New J. Phys.* **17**, 045006 (2015).
- [22] K. Aikawa, A. Frisch, M. Mark, S. Baier, A. Rietzler, R. Grimm, and F. Ferlaino, *Phys. Rev. Lett.* **108**, 210401 (2012).
- [23] S. Baier, M. J. Mark, D. Petter, K. Aikawa, L. Chomaz, Z. Cai, M. Baranov, P. Zoller, and F. Ferlaino, *Science* **352**, 201 (2016).
- [24] C. Ospelkaus, S. Ospelkaus, L. Humbert, P. Ernst, K. Sengstock, and K. Bongs, *Phys. Rev. Lett.* **97**, 120402 (2006).
- [25] J. G. Danzl, E. Haller, M. Gustavsson, M. J. Mark, R. Hart, N. Bouloufa, O. Dulieu, H. Ritsch, and H.-C. Nägerl, *Science* **321**, 1062 (2008).
- [26] K.-K. Ni, S. Ospelkaus, M. H. G. de Miranda, A. Pe'er, B. Neyenhuis, J. J. Zirbel, S. Kotochigova, P. S. Julienne, D. S. Jin, and J. Ye, *Science* **322**, 231 (2008).
- [27] S. Ospelkaus, K.-K. Ni, M. H. G. de Miranda, B. Neyenhuis, D. Wang, S. Kotochigova, P. S. Julienne, D. S. Jin, and J. Ye, *Faraday Disc.* **142**, 351 (2009).
- [28] A. Chotia, B. Neyenhuis, S. A. Moses, B. Yan, J. P. Covey, M. Foss-Feig, A. M. Rey, D. S. Jin, and J. Ye, *Phys. Rev. Lett.* **108**, 080405 (2012).
- [29] A. Frisch, M. Mark, K. Aikawa, S. Baier, R. Grimm, A. Petrov, S. Kotochigova, G. Quémener, M. Lepers, O. Dulieu, and F. Ferlaino, *Phys. Rev. Lett.* **115**, 203201 (2015).
- [30] Z. Idziaszek and P. S. Julienne, *Phys. Rev. Lett.* **104**, 113202 (2010).
- [31] A. Micheli, Z. Idziaszek, G. Pupillo, M. A. Baranov, P. Zoller, and P. S. Julienne, *Phys. Rev. Lett.* **105**, 073202 (2010).
- [32] M. Mayle, B. P. Ruzic, and J. L. Bohn, *Phys. Rev. A* **85**, 062712 (2012).
- [33] M. Mayle, G. Quémener, B. P. Ruzic, and J. L. Bohn, *Phys. Rev. A* **87**, 012709 (2013).
- [34] A. Christianen, T. Karman, and G. C. Groenenboom, *Phys. Rev. A* **100**, 032708 (2019).
- [35] A. Dočaj, M. L. Wall, R. Mukherjee, and K. R. A. Hazzard, *Phys. Rev. Lett.* **116**, 135301 (2016).
- [36] M. L. Wall, N. P. Mehta, R. Mukherjee, S. S. Alam, and K. R. A. Hazzard, *Phys. Rev. A* **95**, 043635 (2017).
- [37] M. L. Wall, R. Mukherjee, S. S. Alam, N. P. Mehta, and K. R. A. Hazzard, *Phys. Rev. A* **95**, 043636 (2017).
- [38] K. D. Ewart, M. L. Wall, and K. R. A. Hazzard, *Phys. Rev. A* **98**, 013611 (2018).
- [39] L. D. Carr, D. DeMille, R. V. Krems, and J. Ye, *New J. Phys.* **11**, 055049 (2009).
- [40] A. V. Gorshkov, S. R. Manmana, G. Chen, E. Demler, M. D. Lukin, and A. M. Rey, *Phys. Rev. A* **84**, 033619 (2011).
- [41] K. R. A. Hazzard, B. Gadway, M. Foss-Feig, B. Yan, S. A. Moses, J. P. Covey, N. Y. Yao, M. D. Lukin, J. Ye, D. S. Jin, and A. M. Rey, *Phys. Rev. Lett.* **113**, 195302 (2014).
- [42] H. Pu, W. Zhang, and P. Meystre, *Phys. Rev. Lett.* **87**, 140405 (2001).
- [43] A. Micheli, G. K. Brennen, and P. Zoller, *Nat. Phys.* **2**, 341 (2006).
- [44] R. Barnett, D. Petrov, M. Lukin, and E. Demler, *Phys. Rev. Lett.* **96**, 190401 (2006).
- [45] A. de Paz, A. Sharma, A. Chotia, E. Maréchal, J. H. Huckans, P. Pedri, L. Santos, O. Gorceix, L. Vernac, and B. Laburthe-Tolra, *Phys. Rev. Lett.* **111**, 185305 (2013).
- [46] G. Mazzarella, S. M. Giampaolo, and F. Illuminati, *Phys. Rev. A* **73**, 013625 (2006).
- [47] O. Dutta, M. Gajda, P. Hauke, M. Lewenstein, D.-S. Lühmann, B. A. Malomed, T. Sowiński, and J. Zakrzewski, *Rep. Prog. Phys.* **78**, 066001 (2015).
- [48] P. Sengupta, L. P. Pryadko, F. Alet, M. Troyer, and G. Schmid, *Phys. Rev. Lett.* **94**, 207202 (2005).

- [49] V. W. Scarola and S. Das Sarma, *Phys. Rev. Lett.* **95**, 033003 (2005).
- [50] D. L. Kovrizhin, G. V. Pai, and S. Sinha, *Europhys. Lett.* **72**, 162 (2005).
- [51] V. W. Scarola, E. Demler, and S. Das Sarma, *Phys. Rev. A* **73**, 051601(R) (2006).
- [52] C. Menotti, C. Trefzger, and M. Lewenstein, *Phys. Rev. Lett.* **98**, 235301 (2007).
- [53] M. Iskin, *Phys. Rev. A* **83**, 051606(R) (2011).
- [54] C. Trefzger, C. Menotti, B. Capogrosso-Sansone, and M. Lewenstein, *J. Phys. B* **44**, 193001 (2011).
- [55] K. Shimizu, T. Hirano, J. Park, Y. Kuno, and I. Ichinose, *New J. Phys.* **20**, 083006 (2018).
- [56] K. Shimizu, T. Hirano, J. Park, Y. Kuno, and I. Ichinose, *Phys. Rev. A* **98**, 063603 (2018).
- [57] O. Tieleman, A. Lazarides, and C. Morais Smith, *Phys. Rev. A* **83**, 013627 (2011).
- [58] C. Zhang, A. Safavi-Naini, A. M. Rey, and B. Capogrosso-Sansone, *New J. Phys.* **17**, 123014 (2015).
- [59] M. Ueda, *Fundamentals and New Frontiers of Bose-Einstein Condensation* (World Scientific, Singapore, 2010).
- [60] D. S. Rokhsar and B. G. Kotliar, *Phys. Rev. B* **44**, 10328 (1991).
- [61] K. Sheshadri, H. R. Krishnamurthy, R. Pandit, and T. V. Ramakrishnan, *Europhys. Lett.* **22**, 257 (1993).
- [62] R. Bai, S. Bandyopadhyay, S. Pal, K. Suthar, and D. Angom, *Phys. Rev. A* **98**, 023606 (2018).
- [63] S. Pal, R. Bai, S. Bandyopadhyay, K. Suthar, and D. Angom, *Phys. Rev. A* **99**, 053610 (2019).
- [64] K. Suthar, R. Bai, S. Bandyopadhyay, S. Pal, and D. Angom, [arXiv:1904.12649](https://arxiv.org/abs/1904.12649).
- [65] C. Trefzger, C. Menotti, and M. Lewenstein, *Phys. Rev. A* **78**, 043604 (2008).
- [66] D. van Oosten, P. van der Straten, and H. T. C. Stoof, *Phys. Rev. A* **63**, 053601 (2001).
- [67] M. Iskin and J. K. Freericks, *Phys. Rev. A* **79**, 053634 (2009).
- [68] J. K. Freericks and H. Monien, *Phys. Rev. B* **53**, 2691 (1996).
- [69] R. Sachdeva and S. Ghosh, *Phys. Rev. A* **85**, 013642 (2012).
- [70] M. Iskin and J. K. Freericks, *Phys. Rev. A* **80**, 063610 (2009).
- [71] T. Sowiński and R. W. Chhajlany, *Phys. Scr.* **T160**, 014038 (2014).
- [72] A. Safavi-Naini, J. von Stecher, B. Capogrosso-Sansone, and S. T. Rittenhouse, *Phys. Rev. Lett.* **109**, 135302 (2012).
- [73] M. Singh, S. Greschner, and T. Mishra, *Phys. Rev. A* **98**, 023615 (2018).
- [74] B. Spivak and S. A. Kivelson, *Phys. Rev. B* **70**, 155114 (2004).
- [75] L. Hruby, N. Dogra, M. Landini, T. Donner, and T. Esslinger, *Proc. Natl. Acad. Sci. USA* **115**, 3279 (2018).
- [76] C. Chin, R. Grimm, P. Julienne, and E. Tiesinga, *Rev. Mod. Phys.* **82**, 1225 (2010).
- [77] J. Werner, A. Griesmaier, S. Hensler, J. Stuhler, T. Pfau, A. Simoni, and E. Tiesinga, *Phys. Rev. Lett.* **94**, 183201 (2005).
- [78] K. Baumann, N. Q. Burdick, M. Lu, and B. L. Lev, *Phys. Rev. A* **89**, 020701(R) (2014).
- [79] A. Frisch, M. Mark, K. Aikawa, F. Ferlaino, J. L. Bohn, C. Makrides, A. Petrov, and S. Kotochigova, *Nature* **507**, 475 (2014).
- [80] T. Maier, H. Kadau, M. Schmitt, M. Wenzel, I. Ferrier-Barbut, T. Pfau, A. Frisch, S. Baier, K. Aikawa, L. Chomaz, M. J. Mark, F. Ferlaino, C. Makrides, E. Tiesinga, A. Petrov, and S. Kotochigova, *Phys. Rev. X* **5**, 041029 (2015).
- [81] L. Bonnes and S. Wessel, *Phys. Rev. Lett.* **106**, 185302 (2011).
- [82] Y.-C. Chen, K.-K. Ng, and M.-F. Yang, *Phys. Rev. B* **84**, 092503 (2011).
- [83] G. Bismut, B. Laburthe-Tolra, E. Maréchal, P. Pedri, O. Gorceix, and L. Vernac, *Phys. Rev. Lett.* **109**, 155302 (2012).
- [84] K. Aikawa, S. Baier, A. Frisch, M. Mark, C. Ravensbergen, and F. Ferlaino, *Science* **345**, 1484 (2014).
- [85] V. Veljić, A. R. P. Lima, L. Chomaz, S. Baier, M. J. Mark, F. Ferlaino, A. Pelster, and A. Balaž, *New J. Phys.* **20**, 093016 (2018).